ANTIOXIDANTS & REDOX SIGNALING
Volume 28, Number 2, 2018

DOI: 10.1089/ars.2017.7106

Therapeutics

ORIGINAL RESEARCH COMMUNICATION

Radiotherapy Synergizes with the Hypoxia-Activated Prodrug Evofosfamide: *In Vitro* and *In Vivo* Studies

Yoichi Takakusagi,[1,2] Shun Kishimoto,[1] Sarwat Naz,[1] Shingo Matsumoto,[1,3] Keita Saito,[1] Charles P. Hart,[4] James B. Mitchell,[1] and Murali C. Krishna[1]

Abstract

Aims: Evofosfamide (TH-302) is a hypoxia-activated prodrug (HAP) that releases the DNA-damaging bromoisophosphoramide mustard (Br-IPM) moiety selectively under hypoxic conditions. Since solid tumors are known to have hypoxic regions, HAPs in combination with chemotherapy or radiotherapy (XRT) will be beneficial. We tested the oxygen dependence of release kinetics of Br-IPM using electron paramagnetic resonance (EPR) with spin trapping by monitoring redox cycling of the nitroimidazole moiety of TH-302, and oxygen dependence of TH-302 on *in vitro* cytotoxicity at different levels of hypoxia was also examined. Two tumor implants (SCCVII and HT29) in mice were studied.

Results: TH-302 fragmentation to release Br-IPM was noticed at oxygen levels <76 mmHg, which increased with higher levels of hypoxia. Enhanced cellular cytotoxicity was also observed at oxygen levels <76 mmHg. *In vivo* pO_2 imaging in the two tumor implants showed that the SCCVII tumor implant had higher level of hypoxia compared with the HT29 xenograft. TH-302 as a monotherapy *in vivo* showed modest effects in SCCVII implants and minimal effects in HT29 xenografts, whereas TH-302 in combination with ionizing radiation showed significant benefit in both tumor models.

Innovation: We examined the kinetics of redox cycling *versus* fragmentation of TH-302. The combination of oxygen-dependent XRT with TH-302 is effective even in tumors with significant hypoxia.

Conclusions: Imaging studies identifying the magnitude of hypoxia in tumors indicated that the responsiveness to TH-302 and the antitumor effect of TH-302 were enhanced by combining with XRT in both the TH-302-sensitive SCCVII tumor and -resistant HT29 tumor. *Antioxid. Redox Signal.* 28, 131–140.

Keywords: EPR, hypoxia, hypoxic cytotoxin, TH-302, radiation

Introduction

SOLID TUMORS comprise structurally and functionally aberrant vasculature compared with normal tissue, which can result in chronic (diffusion-limited) and acute (cycling) hypoxia where pO_2 levels can be below 10 mmHg (7). Several studies using polarographic measurements with Clark-type needle electrodes have shown the presence of hypoxia in several solid tumors (10, 11). Hypoxia has been associated with resistance to radiotherapy (XRT) and chemotherapy. Studies have shown that hypoxia in cancer is associated with decrease in disease-free and overall survival with XRT (4–6). Although proliferating cells in normoxic regions of the tumor respond to XRT or chemotherapy, hypoxic cells can survive the treatment and repopulate, resulting in treatment failure (4).

To achieve improved response in treatment with conventional therapies that are effective in normoxic and proliferating cells in tumors, drugs specifically targeting hypoxic cells have been developed (9, 26). Evofosfamide (TH-302), a hypoxia-activated prodrug (HAP), was developed to selectively target hypoxic regions in tumors and, in preclinical

[1]Radiation Biology Branch, Center for Cancer Research, National Cancer Institute, Bethesda, Maryland.
[2]National Institutes for Quantum and Radiological Science and Technology, Chiba, Japan.
[3]Graduate School of Information Science and Technology, Hokkaido University, Sapporo, Japan.
[4]Threshold Pharmaceuticals, Inc., South San Francisco, California.

Innovation

By using electron paramagnetic resonance (EPR) spin trapping, we clarified the kinetics of redox cycling *versus* fragmentation of evofosfamide (TH-302) to critically evaluate the hypoxia dependence of cytotoxicity. Better understanding of chemical properties of TH-302 will contribute to further development of therapy mode such as combination therapy with radiotherapy (XRT).

studies, it has been shown to improve the overall response when used in combination therapy with antiproliferative agents (14, 19, 21, 22). TH-302 contains a nitroimidazole moiety covalently linked to a bromo-isophosphoramide mustard (Br-IPM) moiety (Fig. 1A) (8). The nitroimidazole moiety can undergo one-electron reduction by intracellular enzymes such as NADPH cytochrome P450 oxidoreductases (PORs) to the corresponding nitro anion radical, which is restored back to its original state at diffusion-limited rate constants in the presence of oxygen (12, 13, 24). With lower concentrations of oxygen, the one-electron reduction product of TH-302 undergoes unimolecular fragmentation at modest rate constants (15) to release the Br-IPM moiety, which is an avid DNA crosslinking agent and can exert significant cytotoxicity (Fig. 1A). Thus, the nitroimidazole moiety in TH-302 serves as an O_2 sensor to release the DNA-alkylating Br-IPM.

Initial reports using TH-302 showed >200-fold enhancement in killing hypoxic *versus* aerobic cells *in vitro* as well as potency in tumor growth inhibition as a monotherapy or in combination chemotherapy (8). TH-302 efficacy has been tested in several cancer cell lines *in vitro* and as xenografts *in vivo* (22). These studies have shown that TH-302 was effective in a variety of tumor types with specificity for hypoxic regions in a tumor and also exhibiting bystander effects (22). Modulating tumor hypoxia by changing the oxygen content in breathing gas had a significant antitumor effect in the combination treatment of TH-302 and single-dose radiation (16). These results supported the notion that HAPs are effective by targeting the tumor microenvironment rather than specific pathways. A detailed *in vitro* study using several cell lines showed that TH-302 displayed a hypoxia cytotoxicity ratio between 550 and 11 (15, 22), the potency being related to the activity of PORs, whereas the molecular mechanisms underlying TH-302 were found to be DNA crosslinking and cell cycle arrest (15).

Combination therapy of TH-302 with several chemotherapy drugs was tested in tumor xenograft studies where TH-302 significantly enhanced the efficacy of antiproliferatives such as gemcitabine, doxorubicin, mTOR inhibitors, chk1 inhibitors, and radiation (8, 9, 14a, 18, 19). It was also shown that pyruvate administration also potentiated TH-302 cytotoxicity by transiently inducing hypoxia (17, 23), while vasodilatory agents such as hydralazine potentiate TH-302 by the so-called steal effect (2). Magnetic resonance imaging (MRI) studies in preclinical xenograft models with dynamic contrast enhancement measuring tumor permeability/perfusion and diffusion-weighted MRI measuring cell density have provided useful imaging biomarkers to monitor treatment response with TH-302 at an early stage (5, 28). It was also found that TH-302 displayed a better safety profile than ifosfamide in preclinical human tumor xenograft models (20).

Based on promising preclinical studies, TH-302 was evaluated for clinical use. The pharmacokinetics, maximal tolerated dose, and dose-limiting toxicities were determined in a phase I study (25). The tolerability of this drug in these studies at the therapeutic doses allowed clinical studies as a monotherapy or combination therapy. A randomized phase II study in 214 patients with locally advanced or metastatic pancreatic cancer using TH-302 in combination with gemcitabine (3) and in combination with doxorubicin in patients with soft tissue sarcoma showed improved tumor response and progression-free survival (6). However, larger phase III studies in advanced pancreatic cancers in combination with gemcitabine or in sarcomas in combination with doxorubicin did not show a statistically significant benefit in terms of overall survival (1). A possible reason for the observed lack of benefit in overall survival in a larger cohort, phase III, may be a selection criterion for the presence of hypoxia for inclusion in the TH-302+gemcitabine treatment in pancreatic cancer or TH-302+doxorubicin in the soft tissue sarcoma study. Although solid tumors are known to have hypoxic regions, the frequency and extent of hypoxia in solid tumors may not depend on tumor size or grade. A recent preclinical study showed that imaging techniques can be used to assess tumor hypoxia and this can predict the outcome in the TH-302 study (18).

The present study was designed to examine the oxygen dependence of redox-activated TH-302 in undergoing fragmentation and release of DNA-alkylating Br-IPM in enzymatic systems. The hypoxic cytotoxicity ratio (HCR) was defined as the TH-302 concentration at 10% cell survival level under aerobic conditions divided by the same survival level of TH-302 concentration at each level of oxygen. HCR of *in vitro* cellular incubations with TH-302 was examined for both SCCVII cells and HT29 cells. Quantitative pO_2 imaging studies using electron paramagnetic resonance (EPR) to profile tumor oxygen status were employed to predict the fragmentation capability of TH-302. By combining these results, we could successfully predict the efficacy of TH-302 treatment on both tumors. The effects of combination therapy with XRT on both tumors were also examined.

Results

To study the redox cycling behavior of TH-302 upon bioreductive activation, EPR spin-trapping studies were conducted in the presence of NADPH (1 m*M*), 4.5 μg/ml POR, and the spin trap dimethylpyrroline N-oxide (DMPO; 110 m*M*) to monitor the steady-state levels of the superoxide adduct of DMPO (Fig. 1B). When the reaction was conducted under aerobic conditions, the superoxide adduct of DMPO, DMPO-OOH, was detected, whereas this adduct was absent in anaerobic conditions (Fig. 1B), suggesting that the TH-302 molecule, even upon being activated, is preserved chemically by redox cycling under aerobic conditions (Fig. 1A). Similar experiments were conducted and the EPR spectra representing the DMPO-superoxide adduct were recorded as a function of time to determine the redox cycling behavior of TH-302 under various levels of dissolved oxygen (Fig. 1C). Under ambient aerobic conditions where the reaction mixture was constantly supplied with room air (150 mmHg O_2), the time course of the DMPO-OOH adduct showed an initial increase, after which a steady state is attained in 2 min and

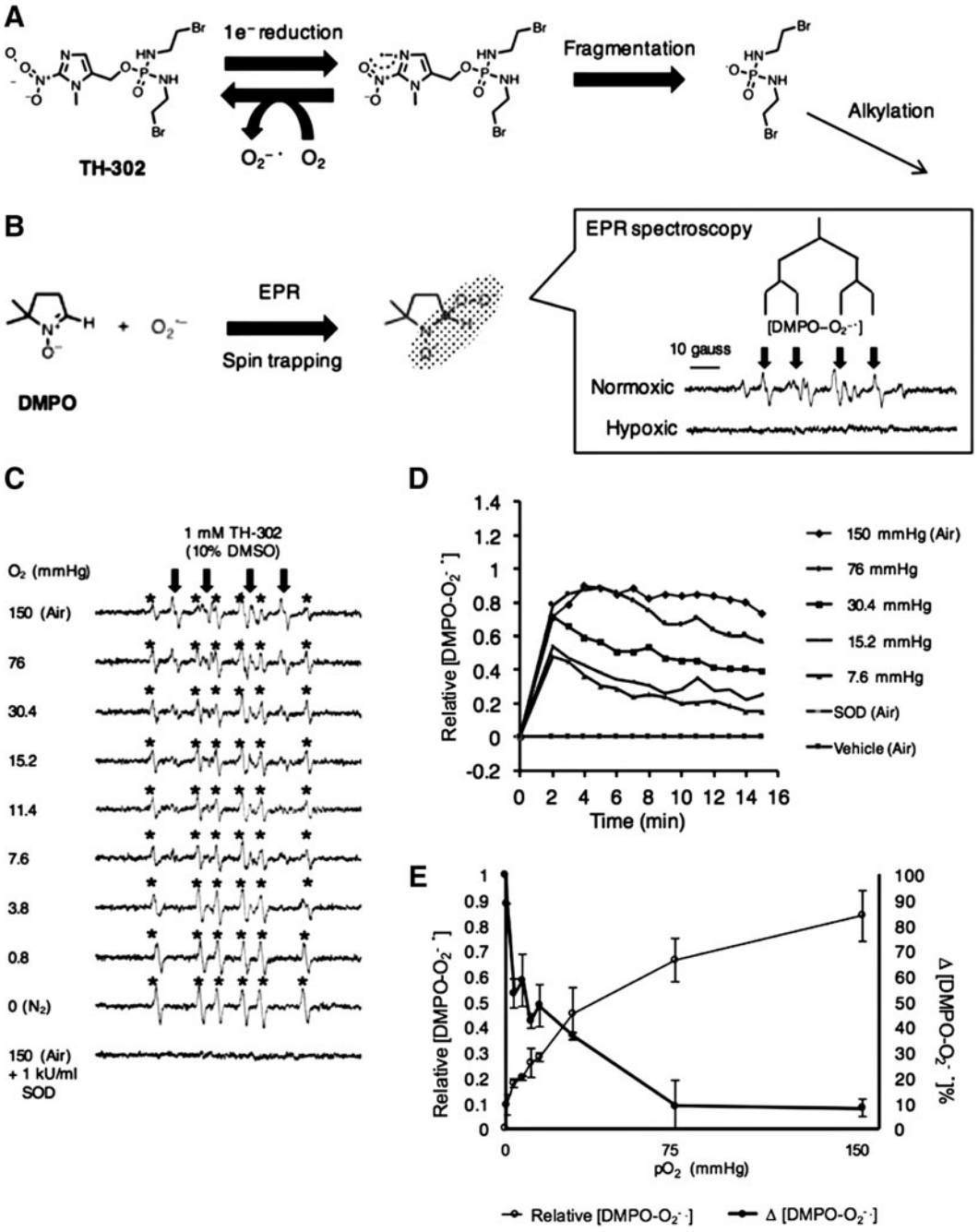

FIG. 1. Spin-trapping EPR spectroscopy. (A) Schema of TH-302 redox cycling under normoxia and fragmentation under hypoxia. **(B)** Spin trapping of superoxide by DMPO (110 m*M*) and the EPR spectra under normoxia or hypoxia. The spin adduct signal [DMPO–$O_2^{-\bullet}$] is indicated by *downward arrows*. Experimental condition; DPBS-10% DMSO containing 1 m*M* NADPH, 4.5 μg/ml POR, and 1 m*M* of TH-302. **(C)** EPR spectra recorded under the indicated oxygen concentration. The spin adduct signal [DMPO–$O_2^{-\bullet}$] formed by PORs during the reduction of TH-302 at 37°C is shown by *downward arrows*. DMPO-CH_3 is indicated by (*). **(D)** A plot of [DMPO–$O_2^{-\bullet}$] signal (every 1 min) recorded for 15 min under the indicated condition of enzymatic reaction at 37°C. **(E)** A plot for the maximum intensity of [DMPO–$O_2^{-\bullet}$] (*open circles*) and the proportion of decline of [DMPO–$O_2^{-\bullet}$] (*closed circles*) at time point of 10 min in Figure 1D. DMPO, dimethylpyrroline N-oxide; DMSO, dimethyl sulfoxide; DPBS, Dulbecco's phosphate-buffered saline; EPR, electron paramagnetic resonance; POR, NADPH cytochrome P450 oxidoreductase.

persisted, suggesting that TH-302, NADPH, and DMPO were not completely consumed. The half-life of DMPO-OOH is ~30 s and its steady state under aerobic conditions suggests that the rates of its production and disappearance are equal, which in turn suggests that the TH-302 levels remain unchanged under aerobic condition *via* futile redox cycling. Another spin adduct attributed to a carbon-centered radical (indicated by *) is also formed. This adduct may result from reduction of adventitious redox-active transition metal complexes (Supplementary Fig. S1; Supplementary Data are

available online at www.liebertpub.com/ars). When the same reaction was conducted at lower concentrations of oxygen (150–0.8 mmHg O_2), the DMPO-OOH adduct reached a peak ~2 min after which its levels decreased (Fig. 1D). However, the DMPO-OOH levels in the reaction at lower levels of O_2 decrease after reaching a peak at 2 min. This pattern suggests that TH-302 must be consumed by fragmentation of the molecule under lower concentrations of oxygen. This can be attributed to a relatively more efficient reaction to release Br-IPM than futile redox cycling at higher levels of oxygen. With decreased oxygen levels, while the time to peak remained the same, the peak levels attained for DMPO-OOH were lower, suggesting that fragmentation of TH-302 was predominant at low levels of oxygen. The results of oxygen dependence of DMPO-OOH steady-state levels are shown in Figure 1E (open circles). From the data shown in Figure 1D, the difference in the peak and plateau levels of DMPO-OOH was determined and plotted in Figure 1E (closed circles). Since the rate of reoxidation of TH-$302^{-\bullet}$ proceeds at rates $>10^8\ M^{-1}s^{-1}$ compared with fragmentation ($130\ s^{-1}$), and further that the DMPO-OOH production and disappearance rates are similar, $[DMPO\text{-}OOH]_{ss}$ can be assumed to be directly proportional to $[TH\text{-}302^{-\bullet}]_{redox\ cycling}$. Furthermore, the difference between [DMPO-OOH] at the peak level and at steady-state level should be related to the fraction of TH-$302^{-\bullet}$, which proceeds through fragmentation to release the alkylating species, $[TH\text{-}302]_{frag}$. Thus, the EPR spin-trapping data from enzymatic incubations of TH-302 show that under hypoxic/anoxic conditions, there is a significant decrease of the steady-state TH-$302^{-\cdot}$ anion radical intermediate implying the facile fragmentation to release the alkylating species. From these enzymatic studies, it can be inferred that there is a strong dependence of TH-302 cytotoxicity to the extent of hypoxia in cells. For example, while under aerobic conditions, negligible loss of TH-302 through fragmentation (no difference in peak and plateau levels of DMPO-OOH) was noticed, and under anoxic conditions, near complete loss of TH-302 was observed since the DMPO-OOH level reached control levels in the absence of TH-302. At 0 mmHg O_2, $[TH\text{-}302^{-\bullet}]_{frag}$ was maximal, and at O_2 levels in the range of 7.6–15.2 mmHg, they dropped by ~50%, suggesting the highly selective release of the alkylating moiety.

The oxygen-dependent cytotoxicity of TH-302 was evaluated using clonogenic cell survival assays in SCCVII and HT29 cells incubated *in vitro*. Figure 2A shows the TH-302 dose-dependent cytotoxicity in SCCVII and HT29 cells under aerobic and hypoxic conditions. At the 10% survival level, TH-302 was effective at 50 μM under aerobic conditions *versus* 40 nM under hypoxic conditions in SCCVII cells. Similarly in HT29 cells, TH-302 was effective at 80 μM under aerobic conditions *versus* 200 nM under hypoxia at the 10% survival level. Results from studies with cellular cytotoxicity assays indicate that there is over a two or a three orders of magnitude higher potency of TH-302 in hypoxia compared with normoxia. Since the range of oxygen levels *in vivo* typically are between 30 and 0 mmHg in normoxia and anoxia/hypoxia, respectively, we conducted studies evaluating the dose dependence of TH-302 cytotoxicity in SCCVII cells incubated at 150, 76, 30.4, 7.6, and 0 mmHg oxygen levels in SCCVII cells and the results are shown in Figure 2B. At the 10% survival level, TH-302 was effective at 50 nM, 200 nM, 1 μM, 10 μM, and 50 μM at oxygen levels of 0, 7.6, 30.4, 76, and 150 mmHg, respectively, clearly suggesting a hypoxia level dependence of TH-302 cytotoxicity. These *in vitro* cell studies further suggested that TH-302 may be efficacious in combination treatments where modalities that are effective against oxygenated fractions of tumors together with a hypoxic cytotoxin can result in an improved outcome. The observed similar profiles of $[TH\text{-}302^{-\bullet}]_{frag}$ and the TH-302 HCR (Fig. 2C) as a function of oxygen levels point to the sharp decline in its potency even at ~10 mmHg. The inverse relationship between the DMPO-OOH levels and TH-302 HCR (Fig. 2C) suggests that reactive oxygen species generation is not related to the hypoxia-specific cytotoxicity of evofosfamide (Supplementary Figs. S2–S4). It also should be noted that SCCVII displayed ~10-fold higher sensitivity to TH-302 than HT29.

A priori assessment of tumor hypoxia will in general be of value in determining treatment outcome. The anatomic images from T_2-weighted MRI scans and the corresponding

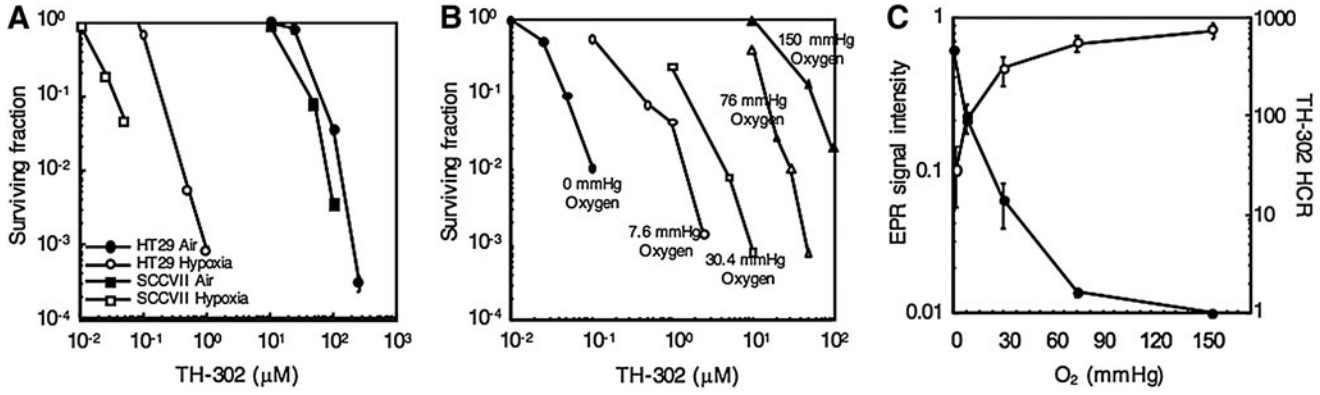

FIG. 2. ***In vitro*** **cell survival assay at various oxygen levels. (A)** Cell survival assay assessed after 2 h of treatment of varying concentrations of TH-302 under aerobic (150 mmHg oxygen) or anoxic (0 mmHg oxygen) conditions on SCCVII and HT29 cells. **(B)** Cell survival assay on SCCVII cells assessed after 2 h of treatment of varying concentrations of TH-302 at various oxygen levels. **(C)** The effect of oxygen levels on toxicity of TH-302 (HCR) and signal intensity as measured by EPR spin-trapping studies shown in Figure 1D and E. TH-302 HCR was determined from three experiments; error bars represent the SE. HCR, hypoxic cytotoxicity ratio; SE, standard error.

EPR-based pO_2 maps in SCCVII and HT29 tumor implants in mice are shown in Figure 3A. From the quantitative analysis of each tumor oxygen pressure, median pO_2 in SCCVII ($\sim 980\,mm^3$) was 10.9 ± 1.0 mmHg ($n=3$) on average, while 14.5 ± 0.8 mmHg ($n=4$) was calculated from HT29 tumor pO_2 maps ($\sim 650\,mm^3$) (Fig. 3B). The hypoxic fraction (HF) of <15.2 or 10 mmHg in each tumor, calculated from the pO_2 maps, was $79.8\% \pm 6.1\%$, $50.1\% \pm 6.7\%$ in the SCCVII tumor and $52.8\% \pm 6.4\%$, $24.3\% \pm 5.5\%$ in the HT29 tumor, respectively (Fig. 3C). These results indicate that the tumor oxygen level in SCCVII tumors is lower than that of HT29. The pO_2 maps show that the SCCVII tumor implant displays significant hypoxia ($pO_2 < 10$ mmHg) and significant spatial heterogeneity, while the HT29 tumor xenograft displays a hypoxic core surrounded by well-oxygenated regions. These differences are consistent with those from previous studies where histological studies revealed that the HT29 vasculature was structurally more robust than that of the SCCVII tumor (27). These results predict that HT29 is theoretically resistant to TH-302 treatment in terms of not only cellular sensitivity but also tumor hypoxia profile, whereas SCCVII is theoretically sensitive. The treatment with HAPs such as TH-302 may result in treatment failure in HT29 due to repopulation of aerobic fractions where not HAP, but XRT is effective.

To evaluate the efficacy of TH-302 either as a monotherapy or in combination with XRT, SCCVII and HT29 xenografts were studied in normal competent mice and athymic nude mice, respectively. The choice of these cells was based on our prior studies where the SCCVII tumor implants showed both acutely hypoxic (cycling hypoxia) and chronically hypoxic regions (diffusion-limited hypoxia), whereas the HT29 tumor xenografts showed acute hypoxia to a lesser extent, but had regions of chronic hypoxia in addition to cellular sensitivity to TH-302 examined in Figure 2 (27). Therefore, differences in TH-302 cellular sensitivities, tumor microenvironments, and tumor hypoxia profiles served as SCCVII tumor for TH-302 sensitive and HT29 tumor for TH-302 resistant. TH-302 effectiveness as a monotherapy or in combination with fractionated XRT was examined. SCCVII and HT29 tumors were implanted in groups of mice and the tumor growth kinetics was monitored. Figures 4A and B show the tumor doubling time of SCCVII (A) and HT29 (B) tumors in mice treated five times with TH-302 or XRT (3 Gy) alone, or their combination. The corresponding Kaplan–Meier plots are shown in Figure 4C and D. Compared with control, TH-302 as a monotherapy was modestly effective in SCCVII ($p=0.10$), whereas XRT alone had no effect, which is consistent with the hypoxic nature of this tumor. Both XRT and TH-302 as monotherapies had no observable benefit in HT29 xenograft. However, the combination of TH-302 with XRT significantly enhanced the antitumor effect in both SCCVII ($p=0.007$ *vs.* control) and HT29 ($p=0.003$), suggesting that both aerobic and HF of the tumor need to be targeted for a better treatment outcome. These studies suggest that the combination treatment of TH-302 with fractionated XRT is effective in response to treatment compared with TH-302 as a monotherapy.

For a better understanding of the molecular basis of cytotoxicity of TH-302 monotherapy and its combination therapy with XRT, histochemical analyses of the SCCVII tumors treated with each therapy were performed. Figure 5A represents double staining of the hypoxic area (green) and histone γ-H2AX-positive cells (red). Pimonidazole was stained in the hypoxic area and γ-H2AX was in the area where DNA damage occurred since it reflects S139 phosphorylation ($pSer^{139}$). The magnitude of DNA damage was separately assessed based on the pimonidazole-positive/negative area. XRT induced a similar level of DNA damage in both pimonidazole (+) and pimonidazole (−) areas, whereas TH-302 monotherapy and TH-302+XRT induced increased damage preferentially in the pimonidazole (+) area. This observation is consistent with the mechanistic scheme and previous reports (16a). Decreased pimonidazole (+) area was observed only in tumor sections corresponding to TH-302 and XRT combination therapy (Fig. 5B, E), suggesting that decreased cell viability in these regions can result in pimonidazole insensitivity in agreement with an earlier report (16a). Tissue necrosis was also evaluated by hematoxylin and eosin (HE) staining (Fig. 5C). Figure 5F shows the proportion of necrotic area calculated from the HE staining

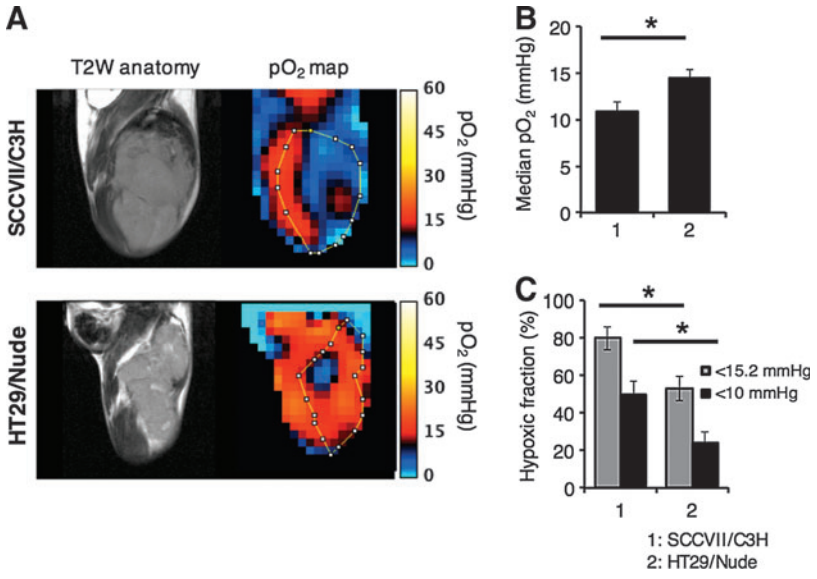

FIG. 3. EPRI/MRI in SCCVII ($n=3$) and HT29 tumors ($n=4$). **(A–C)** Noninvasive monitoring and quantification of tumor median pO_2 by EPR oximetry. **(A)** T_2-weighted anatomical images and pO_2 maps of SCCVII or HT29 ($\sim 800\,mm^3$). **(B, C)** Changes in median pO_2 **(B)** and proportional hypoxic regions **(C)**. Each value was measured across three 2-mm slices. $^*p<0.05$. EPRI, electron paramagnetic resonance imaging; MRI, magnetic resonance imaging.

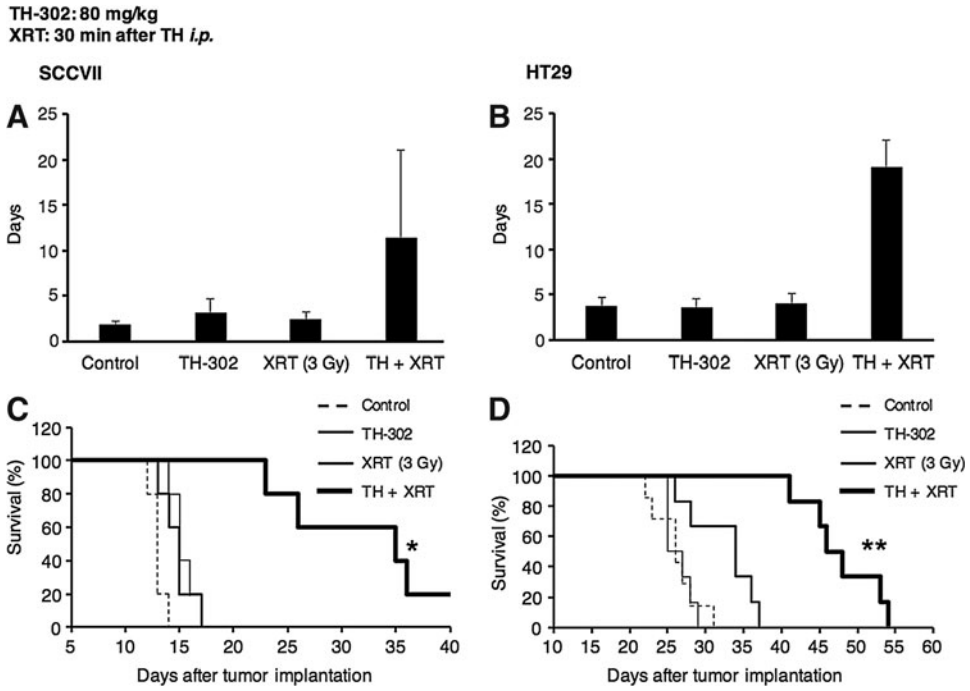

FIG. 4. *In vivo* tumor growth assay. (A, B) Tumor growth assessed by doubling time in size after five times of treatment with TH-302 and/or XRT (3 Gy) on SCCVII tumor-bearing C3H/HeN mice **(A)** and HT29 tumor-bearing athymic nude mice **(B)**. **(C, D)** Kaplan–Meier plot of SCCVII/C3H **(C)** and HT29/nude mice **(D)**. Mice were sacrificed when the tumor volume reached 2000 mm^3. Data are mean ± SE of five **(A, C)** or five to seven **(B, D)** mice. $*p < 0.05$, $**p < 0.001$. XRT, radiotherapy.

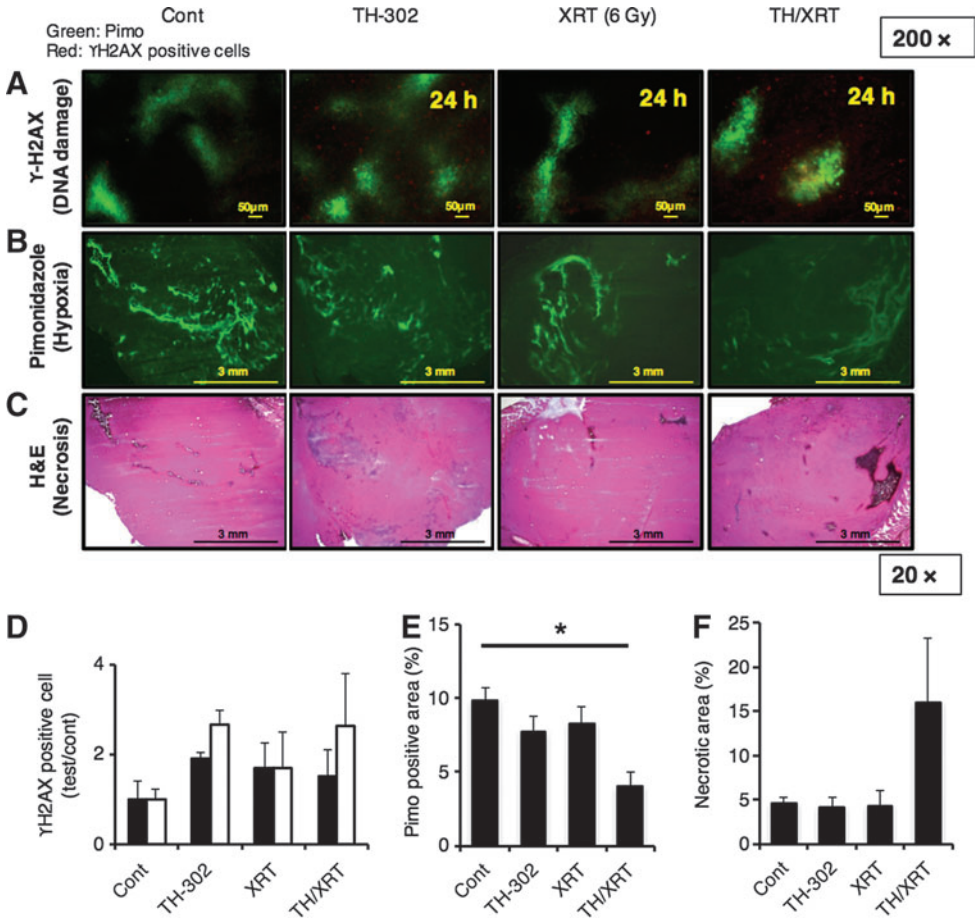

FIG. 5. Histochemical analysis of SCCVII tumor sections 24 h after treatment with TH-302 and/or XRT (6 Gy). ($n = 4$ for the TH-302/XRT group, $n = 3$ for other groups) **(A, B).** Detection of hypoxic area by pimonidazole (pimo) **(A, B)** or DNA damage (γ-H2AX-positive cells) by anti-H2AX ($pSer^{139}$) antibody **(A)**. **(C)** Detection of necrotic area (HE). **(D)** Quantification of γ-H2AX-positive cells at indicated conditions. *Black bar*, pimo-negative area; *white bar*, pimo-positive area. **(E)** Quantification of pimo-positive area at indicated conditions. $*p = 0.006$. **(F)** Quantification of necrotic area at indicated conditions calculated from HE staining. The values shown are mean ± SE from at least three mice. HE, hematoxylin and eosin.

data. The combination therapy induced an approximately threefold larger necrotic area compared with TH-302 monotherapy or XRT. Taken together, the combination of TH-302 with XRT induced tumor necrosis predominantly in the hypoxic region, resulting in a synergistic antitumor effect with XRT, which is effective in the nonhypoxic region.

Discussion

TH-302 is activated by intracellular PORs at the nitroimidazole moiety to the corresponding anion radical (13). This study evaluated the dependence of oxygen levels on the fragmentation pathway, releasing Br-IPM (hypoxic cytotoxicity) *versus* redox cycling under aerobic conditions (Fig. 1A). Enzymatic incubations of TH-302 to detect steady-state levels of the superoxide adduct (DMPO-OOH) of the spin trap DMPO at different conditions of dissolved oxygen were used to estimate the redox cycling of TH-302$^{-\bullet}$, [TH-302$^{-\bullet}$]$_{\text{redox cycling}}$, *versus* its fragmentation, [TH-302$^{-\bullet}$]$_{\text{frag.}}$. The EPR spin-trapping technique is best suited since the superoxide generated by redox cycling of TH-302$^{-\bullet}$ is labile with a half-life of approximately microseconds. DMPO stabilizes the superoxide by forming a covalent adduct, DMPO-OOH, which has a relatively longer half-life of $\sim$30 s in aqueous solutions. In enzymatic systems where superoxide generation and destruction of DMPO-OOH are equal (17a, 17b), the steady-state level of DMPO-OOH can reflect the steady-state concentration of TH-302$^{-\bullet}$. Spin traps such as DEPMPO, EMPO, and BMPO can be used to detect superoxide and the corresponding adducts that have longer half-lives in the order of minutes and in enzymatic incubations and their concentrations increase with time (1a, 2a). However, to monitor levels of TH-302$^{-\bullet}$ at different levels of dissolved oxygen, DMPO is ideal as steady-state levels of DMPO-OOH more closely reflect [TH-302$^{-\bullet}$]$_{\text{redox cycling}}$. EPR spin-trapping studies show that redox-activated TH-302 undergoes facile redox cycling at diffusion-limited rate constants ($\sim 10^9\ M^{-1}s^{-1}$) under aerobic conditions and the molecule is restored to its native form, preserving the Br-IPM intact. However, under decreasing levels of oxygen from 150 mmHg, the steady-state levels of DMPO-OOH decreased, suggesting that the fragmentation pathway even with a lower rate constant ($\sim 130\ s^{-1}$) becomes relevant (15). Figure 1E shows that at lower levels of oxygen, the DMPO-OOH steady-state level reaches a peak and a steady state, which is lower than that under aerobic conditions. The difference between the peak level of DMPO-OOH (at 1-min time point) and its steady-state level (at 10-min time point) reflects the fraction of TH-302$^{-\bullet}$ proceeding toward fragmentation that can potentially lead to DNA alkylation and cell kill. A similar profile of the HCR of TH-302 in SCCVII cells (Fig. 2C, closed circles) and [TH-302$^{-\bullet}$]$_{\text{frag}}$ in enzymatic incubations (Fig. 1E, closed circles) was observed. These results show that TH-302 is effective in extremely hypoxic regions and the presence of oxygen significantly diminishes the potency of TH-302 cytotoxicity. These results also show the $\sim$10-fold higher toxicity of TH-302 on SCCVII cells compared with HT29 cells. Although we used enough amount of PORs to activate TH-302 in the enzymatic experiments in Figure 1 to focus on the effect of hypoxia on the balance between redox cycling and fragmentation, the activity of PORs in tumor cells differs depending on cell lines. Meng *et al.* reported that higher POR expression is associated with higher cytotoxicity (15). This implies that the redox state of cells can influence the activation of TH-302 leading to different cytotoxicity.

The critical dependence of hypoxia on TH-302 cytotoxicity points to a need of using quantitative pO_2 assessment in tumors in formulation of therapies with HAPs in general and TH-302 in particular. EPR imaging is a useful oxygen imaging technique where *in vivo* oxygen determinations can be measured noninvasively and quantitatively (17, 23, 27). EPR imaging with OX063 as a paramagnetic tracer has been shown to be effective in providing quantitative imaging of tumor pO_2 and probing the dynamic fluctuations of tumor pO_2. The two tumor models chosen for this study have significant differences in the tumor microenvironment (27). Although both tumors have significant hypoxia, the contributions of chronic and acute hypoxia are different. Furthermore, the microvasculature differences in terms of pericyte coverage are different with the HT29 tumor vasculature being more robust than that in SCCVII tumor. Combined with the *in vitro* result of TH-302 cytotoxicity showing higher sensitivity in SCCVII cells, the SCCVII tumor and HT29 tumor were predicted as TH-302-responsive tumor and -resistant tumor, respectively. This prediction was supported by Figure 3, which shows the *in vivo* treatment response to TH-302. Figure 3 also showed significant benefit of the combination therapy with XRT in both TH-302-sensitive and -resistant tumors pointing to the importance of targeting proliferating (target of XRT therapy) as well as hypoxic regions (target of TH-302 therapy) in a tumor.

Several preclinical models showed that TH-302 provides significant advantage as combination therapy with antiproliferative agents such as gemcitabine, doxorubicin, topotecan, and mTOR inhibitors (8, 9, 18, 19). However, phase III trials did not reach a statistically significant endpoint in pancreatic carcinomas and sarcomas (1). While in general solid tumors can contain hypoxic regions, it is not uniformly the case. The magnitude of hypoxia ($pO_2 < 10$ mmHg) and the fractional volume in the tumor having hypoxia may differ. Imaging techniques that can provide a semiquantitative assessment of hypoxia may aid in the selection of patients for therapy, including those for HAPs such as TH-302.

In conclusion, our enzymatic studies under well-defined conditions show the dependence of oxygen in determining the fraction of the redox-activated TH-302 proceeding toward fragmentation to release Br-IPM to elicit toxicity. This was directly correlated with the HCR in SCCVII cells *in vitro*. EPR imaging studies show that the two tumors had significant HF of <15.2 mmHg (>50%), yet TH-302 as a monotherapy was not effective, whereas in combination with fractionated XRT, a significant improvement was observed.

Materials and Methods

EPR spin trapping

Reaction mixtures (Dulbecco's phosphate-buffered saline [DPBS]-10% dimethyl sulfoxide [DMSO]) containing 4.5 μg/ml POR (Thermo Fisher), 1 m*M* NADPH, 110 m*M* DMPO, and 1 m*M* TH-302 were transferred to a gas-permeable Teflon capillary (Zeus Industries, Orangeburg, SC) having an inner diameter of 0.81 mm, a wall thickness of 0.38 mm, and a length of 15 cm. Each capillary was folded

twice, inserted into a narrow quartz tube that was open on both ends (2.5 mm inner diameter), and placed within the EPR cavity where O_2 gas heated at 37°C was blown. EPR spectra were recorded using a Varian E-9 X-band spectrometer operating at 9.4 GHz. The modulation amplitude was kept at 1.0 G, and the microwave power at 10 mW.

Cell survival studies

Murine squamous cell carcinoma (SCCVII) cells were derived from established SCCVII tumors (obtained from Dr. T. Phillips, UCSF, San Francisco, CA). The human colon cancer cell line HT29 was purchased from American Type Culture Collection (ATCC). Both cells were tested in 2013 by IDEXX RADIL (Columbia, MO) using a panel of microsatellite markers. All cell lines were grown in RPMI 1640 supplemented with 10% fetal calf serum and antibiotics. The survival of cells exposed to TH-302 and/or XRT under different percentages of oxygen was assessed by clonogenic assays using specially designed glass flasks. Cells (2.5×10^5) were dispersed in 1.8 ml of medium, plated into glass flasks, and incubated at 37°C overnight. Each flask was equipped with a ground-glass sidearm vessel, which when rotated and inverted, could deliver 0.2 ml of medium containing varying concentrations of TH-302. The flasks were then sealed with soft rubber stoppers, and l9-gauge needles were pushed through the rubber stopper to provide entrance and exit ports for a humidified gas mixture of 5% CO_2, 74–95% nitrogen, and varying concentrations of oxygen (0–21%; Matheson Gas Products). The stoppered flasks were connected in series, mounted on a reciprocating platform, and gassed at 37°C for 60 min. The gassing procedure resulted in equilibrium between the gas and liquid phases in the flask as well as the solution in the sidearm. After 60 min of gassing, the sidearm containing the TH-302 solution was inverted, delivering the contents to the cell monolayer. The gassing and drug exposure were continued for 2 h. Cells were then rinsed, trypsinized, counted, plated, and incubated for 10–14 days for macroscopic colony formation. Colonies were fixed with methanol/acetic acid (3:1) and stained with crystal violet. Colonies with >50 cells were scored and cell survival was determined. Experiments were repeated two to three times and the error bars shown in the figures represent the standard error of the mean and are shown when larger than the symbol. HCR, defined as the TH-302 concentration under aerobic conditions divided by the TH-302 concentration at each level of oxygen, was determined at the 10% cell survival level.

Animal studies

All animal experiments were carried out in compliance with the *Guide for the Care and Use of Laboratory Animals* (15a) and approved by the National Cancer Institute (NCI) Animal Care and Use Committee. Female 5–8-week-old C3H/HeN mice (15–23 g) and athymic nude mice (19–27 g) were supplied by the Frederick Cancer Research Center, Animal Production Department. Mouse SCCVII and human HT29 solid tumor formation and management of mice during imaging were carried out as described previously (17, 27). The 80 mg TH-302 (Threshold Pharmaceuticals, Inc.) per kg body weight (80 mg/kg) dissolved in DPBS was intraperitoneally injected, and X-ray (3 Gy) was then irradiated for tumor-bearing mice 30 min after TH-302 administration. Treatment was performed five times on days 7–11 (SCCVII) or days 8–12 (HT29) after tumor implantation.

EPRI and MRI

Technical details of the EPR scanner operating at 300 MHz, data acquisition based on the single-point imaging modality, image reconstruction, and the oxygen mapping procedure were described in earlier reports (17, 23, 27). The electron paramagnetic resonance imaging (EPRI) in SCCVII or HT29 xenograft ($\sim 800\ mm^3$) was carried out according to our previous report (23, 27). MRI scans were conducted using a 7T scanner controlled with ParaVision 5.1 (Bruker BioSpin MRI GmbH). T_2*-weighted anatomic images were obtained. The parameters were calculated using code written in MATLAB (MathWorks).

Histochemical analysis

Tumor tissues were excised 1 h after intravenous injection of pimonidazole, in accordance with the manufacturer's instructions. The tumors frozen by ultracold ethanol (EtOH) were sectioned (10 μm thick) using a cryostat, and sections were thaw-mounted on glass slides. After fixing with 4% paraformaldehyde, sections were treated with cold acetone for 15 min. After blocking nonspecific binding sites on sections with Protein Block Serum-Free reagent (Dako North America, Inc., Carpinteria, CA) for 30 min, the slides were submerged in Mayer's hematoxylin solution (Sigma-Aldrich) for 5 min. After rinsing with water for 20 min, sections were incubated with Eosin Y for 2 min and washed with 80% and 100% EtOH for 5 min each and finally treated with xylene for 5 min. As for the immunohistochemical analysis, the slides were submerged in Rb PhosphoDetect™ Anti-H2AX ($pSer^{139}$) antibody (1:800; Calbiochem) and Hypoxyprobe 4.3.11.3 mouse MAb (1:100; hpi) for pimonidazole staining overnight at 4°C. The sections were then incubated with Alexa Fluor 546 $F(ab')_2$ fragment of goat anti-rabbit IgG (H+L; 1:2000; Invitrogen) for 1 h at room temperature and then mounted with Prolong Gold antifade reagent with DAPI (Invitrogen). Fluorescence microscopy was performed using a BZ-9000 BIOREVO (KEYENCE), and images were captured using the BZ-9000E viewer. To quantify the pimonidazole-positive area and necrotic area, digital images of stained sections at 10× magnification were assembled using the BZ-II Analyzer (KEYENCE) to compose a whole tumor image, and pixels on the positive area were counted. As for evaluation of drug-induced DNA damage, the number of anti-H2AX ($pSer^{139}$) antibody-positive cells in the optical field was counted and converted into numbers per square millimeter of pimonidazole-positive hypoxic area, or other area, respectively ($n = 3$).

Statistical analyses

Welch' s two-sample *t* tests were performed to examine the synergistic effect of XRT and TH-302, and log-rank tests were performed to examine the difference in distribution of survival curves. All statistical analyses were performed using software R (version 3.2.1). One case of tumor disappearance observed in the combination therapy group in SCCVII tumor

was omitted from the bar graph in Figure 3A. Statistical significance was set at $p = 0.05$.

Acknowledgment

This research was supported by the Intramural Research Program of the Center of Cancer Research, NCI, National Institutes of Health.

Author Disclosure Statement

No competing financial interests exist.

References

1. MAESTRO trial of evofosfamide/gemcitabine in PDAC fails to improve OS. *ASCO Press Release.* 2016. http://gicasym.org/maestro-trial-evofosfamidegemcitabine-pdac-fails-improve-os (accessed January 23, 2016).

1a. Abbas K, Hardy M, Poulhes F, Karoui H, Tordo P, Ouari O, and Peyrot F. Detection of superoxide production in stimulated and unstimulated living cells using new cyclic nitrone spin traps. *Free Radic Biol Med* 71: 281–290, 2014.

2. Bailey KM, Cornnell HH, Ibrahim-Hashim A, Wojtkowiak JW, Hart CP, Zhang X, Leos R, Martinez GV, Baker AF, and Gillies RJ. Evaluation of the ''steal'' phenomenon on the efficacy of hypoxia activated prodrug TH-302 in pancreatic cancer. *PLoS One* 9: e113586, 2014.

2a. Beziere N, Hardy M, Poulhes F, Karoui H, Tordo P, Ouari O, Frapart YM, Rockenbauer A, Boucher JL, Mansuy D, and Peyrot F. Metabolic stability of superoxide adducts derived from newly developed cyclic nitrone spin traps. *Free Radic Biol Med* 67: 150–158, 2014.

3. Borad MJ, Reddy SG, Bahary N, Uronis HE, Sigal D, Cohn AL, Schelman WR, Stephenson J, Jr, Chiorean EG, Rosen PJ, Ulrich B, Dragovich T, Del Prete SA, Rarick M, Eng C, Kroll S, and Ryan DP. Randomized phase II trial of gemcitabine plus TH-302 versus gemcitabine in patients with advanced pancreatic cancer. *J Clin Oncol* 33: 1475–1481, 2015.

4. Brizel DM, Dodge RK, Clough RW, and Dewhirst MW. Oxygenation of head and neck cancer: Changes during radiotherapy and impact on treatment outcome. *Radiother Oncol* 53: 113–117, 1999.

5. Cardenas-Rodriguez J, Li Y, Galons JP, Cornnell H, Gillies RJ, Pagel MD, and Baker AF. Imaging biomarkers to monitor response to the hypoxia-activated prodrug TH-302 in the MiaPaCa2 flank xenograft model. *Magn Reson Imaging* 30: 1002–1009, 2012.

6. Chawla SP, Cranmer LD, Van Tine BA, Reed DR, Okuno SH, Butrynski JE, Adkins DR, Hendifar AE, Kroll S, and Ganjoo KN. Phase II study of the safety and antitumor activity of the hypoxia-activated prodrug TH-302 in combination with doxorubicin in patients with advanced soft tissue sarcoma. *J Clin Oncol* 32: 3299–3306, 2014.

7. Dewhirst MW. Relationships between cycling hypoxia, HIF-1, angiogenesis and oxidative stress. *Radiat Res* 172: 653–665, 2009.

8. Duan JX, Jiao H, Kaizerman J, Stanton T, Evans JW, Lan L, Lorente G, Banica M, Jung D, Wang J, Ma H, Li X, Yang Z, Hoffman RM, Ammons WS, Hart CP, and Matteucci M. Potent and highly selective hypoxia-activated achiral phosphoramidate mustards as anticancer drugs. *J Med Chem* 51: 2412–2420, 2008.

9. Foehrenbacher A, Secomb TW, Wilson WR, and Hicks KO. Design of optimized hypoxia-activated prodrugs using pharmacokinetic/pharmacodynamic modeling. *Front Oncol* 3: 314, 2013.

10. Hockel M, Knoop C, Schlenger K, Vorndran B, Baussmann E, Mitze M, Knapstein PG, and Vaupel P. Intratumoral pO_2 predicts survival in advanced cancer of the uterine cervix. *Radiother Oncol* 26: 45–50, 1993.

11. Hockel M, Knoop C, Schlenger K, Vorndran B, Knapstein PG, and Vaupel P. Intratumoral pO_2 histography as predictive assay in advanced cancer of the uterine cervix. *Adv Exp Med Biol* 345: 445–450, 1994.

12. Hunter FW, Wang J, Patel R, Hsu HL, Hickey AJ, Hay MP, and Wilson WR. Homologous recombination repair-dependent cytotoxicity of the benzotriazine di-N-oxide CEN-209: Comparison with other hypoxia-activated prodrugs. *Biochem Pharmacol* 83: 574–585, 2012.

13. Hunter FW, Young RJ, Shalev Z, Vellanki RN, Wang J, Gu Y, Joshi N, Sreebhavan S, Weinreb I, Goldstein DP, Moffat J, Ketela T, Brown KR, Koritzinsky M, Solomon B, Rischin D, Wilson WR, and Wouters BG. Identification of P450 oxidoreductase as a major determinant of sensitivity to hypoxia-activated prodrugs. *Cancer Res* 75: 4211–4223, 2015.

14. Liu Q, Sun JD, Wang J, Ahluwalia D, Baker AF, Cranmer LD, Ferraro D, Wang Y, Duan JX, Ammons WS, Curd JG, Matteucci MD, and Hart CP. TH-302, a hypoxia-activated prodrug with broad in vivo preclinical combination therapy efficacy: Optimization of dosing regimens and schedules. *Cancer Chemother Pharmacol* 69: 1487–1498, 2012.

14a. Meng F, Bhupathi D, Sun JD, Liu Q, Ahluwalia D, Wang Y, Matteucci, MD, and Hart CP. Enhancement of hypoxia-activated prodrug TH-302 anti-tumor activity by Chk1 inhibition. *BMC Cancer* 15: 422, 2015.

15. Meng F, Evans JW, Bhupathi D, Banica M, Lan L, Lorente G, Duan JX, Cai X, Mowday AM, Guise CP, Maroz A, Anderson RF, Patterson AV, Stachelek GC, Glazer PM, Matteucci MD, and Hart CP. Molecular and cellular pharmacology of the hypoxia-activated prodrug TH-302. *Mol Cancer Ther* 11: 740–751, 2012.

15a. National Research Council. Guide for the care and use of laboratory animals. Washington DC: National Academy Press, 1996.

16. Peeters SG, Zegers CM, Biemans R, Lieuwes NG, van Stiphout RG, Yaromina A, Sun JD, Hart CP, Windhorst AD, van Elmpt W, Dubois LJ, and Lambin P. TH-302 in combination with radiotherapy enhances the therapeutic outcome and is associated with pretreatment [18F]HX4 hypoxia PET imaging. *Clin Cancer Res* 21: 2984–2992, 2015.

16a. Saggar JK and Tannock IF. Chemotherapy rescues hypoxic tumor cells and induces their reoxygenation and repopulation-an effect that is inhibited by the hypoxia-activated prodrug TH-302. *Clin Cancer Res* 2: 2107–2114, 2015.

17. Saito K, Matsumoto S, Devasahayam N, Subramanian S, Munasinghe JP, Morris HD, Lizak MJ, Ardenkjaer-Larsen JH, Mitchell JB, and Krishna MC. Transient decrease in tumor oxygenation after intravenous administration of pyruvate. *Magn Reson Med* 67: 801–807, 2012.

17a. Samuni A, Black CD, Krishna CM, Malech HL, Bernstein EF, and Russo A. Hydroxyl radical production by stimulated neutrophils reappraised. *J Biol Chem* 263: 13797–13801, 1988.

17b. Samuni A, Krishna CM, Riesz P, Finkelstein E, and Russo A. Superoxide reaction with nitroxide spin-adducts. *Free Radic Biol Med* 6: 141–148, 1989.

18. Stokes AM, Hart CP, and Quarles CC. Hypoxia imaging with PET correlates with antitumor activity of the hypoxia-

activated prodrug evofosfamide (TH-302) in rodent glioma models. *Tomography* 2: 229–237, 2016.
19. Sun JD, Ahluwalia D, Liu Q, Li W, Wang Y, Meng F, Bhupathi D, Matteucci MD, and Hart CP. Combination treatment with hypoxia-activated prodrug evofosfamide (TH-302) and mTOR inhibitors results in enhanced anti-tumor efficacy in preclinical renal cell carcinoma models. *Am J Cancer Res* 5: 2139–2155, 2015.
20. Sun JD, Liu Q, Ahluwalia D, Ferraro DJ, Wang Y, Jung D, Matteucci MD, and Hart CP. Comparison of hypoxia-activated prodrug evofosfamide (TH-302) and ifosfamide in preclinical non-small cell lung cancer models. *Cancer Biol Ther* 17: 371–380, 2016.
21. Sun JD, Liu Q, Ahluwalia D, Li W, Meng F, Wang Y, Bhupathi D, Ruprell AS, and Hart CP. Efficacy and safety of the hypoxia-activated prodrug TH-302 in combination with gemcitabine and nab-paclitaxel in human tumor xenograft models of pancreatic cancer. *Cancer Biol Ther* 16: 438–449, 2015.
22. Sun JD, Liu Q, Wang J, Ahluwalia D, Ferraro D, Wang Y, Duan JX, Ammons WS, Curd JG, Matteucci MD, and Hart CP. Selective tumor hypoxia targeting by hypoxia-activated prodrug TH-302 inhibits tumor growth in preclinical models of cancer. *Clin Cancer Res* 18: 758–770, 2012.
23. Takakusagi Y, Matsumoto S, Saito K, Matsuo M, Kishimoto S, Wojtkowiak JW, DeGraff W, Kesarwala AH, Choudhuri R, Devasahayam N, Subramanian S, Munasinghe JP, Gillies RJ, Mitchell JB, Hart CP, and Krishna MC. Pyruvate induces transient tumor hypoxia by enhancing mitochondrial oxygen consumption and potentiates the anti-tumor effect of a hypoxia-activated prodrug TH-302. *PLoS One* 9: e107995, 2014.
24. Wardman P, Dennis MF, Everett SA, Patel KB, Stratford MR, and Tracy M. Radicals from one-electron reduction of nitro compounds, aromatic N-oxides and quinones: The kinetic basis for hypoxia-selective, bioreductive drugs. *Biochem Soc Symp* 61: 171–194, 1995.
25. Weiss GJ, Infante JR, Chiorean EG, Borad MJ, Bendell JC, Molina JR, Tibes R, Ramanathan RK, Lewandowski K, Jones SF, Lacouture ME, Langmuir VK, Lee H, Kroll S, and Burris HA, 3rd. Phase 1 study of the safety, tolerability, and pharmacokinetics of TH-302, a hypoxia-activated prodrug, in patients with advanced solid malignancies. *Clin Cancer Res* 17: 2997–3004, 2011.
26. Wilson WR and Hay MP. Targeting hypoxia in cancer therapy. *Nat Rev Cancer* 11: 393–410, 2011.
27. Yasui H, Matsumoto S, Devasahayam N, Munasinghe JP, Choudhuri R, Saito K, Subramanian S, Mitchell JB, and Krishna MC. Low-field magnetic resonance imaging to visualize chronic and cycling hypoxia in tumor-bearing mice. *Cancer Res* 70: 6427–6436, 2010.
28. Zhang X, Wojtkowiak JW, Martinez GV, Cornnell HH, Hart CP, Baker AF, and Gillies R. MR imaging biomarkers to monitor early response to hypoxia-activated prodrug TH-302 in pancreatic cancer xenografts. *PLoS One* 11: e0155289, 2016.

Address correspondence to:
Dr. Murali C. Krishna
Radiation Biology Branch
Center for Cancer Research
National Cancer Institute
Bldg. 10, Room B3-B69
Bethesda, MD 20892

E-mail: cherukum@mail.nih.gov

Date of first submission to ARS Central, April 6, 2017; date of final revised submission, July 14, 2017; date of acceptance, July 22, 2017.

Abbreviations Used

Br-IPM = bromo-isophosphoramide mustard
DMPO = dimethylpyrroline N-oxide
DPBS = Dulbecco's phosphate-buffered saline
EPR = electron paramagnetic resonance
EtOH = ethanol
HAP = hypoxia-activated prodrug
HCR = hypoxic cytotoxicity ratio
HE = hematoxylin and eosin
HF = hypoxic fraction
MRI = magnetic resonance imaging
PORs = NADPH cytochrome P450 oxidoreductases
XRT = radiotherapy